High Heat-Flux Heat Transfer and Pressure Drop Correlations for Reactor Thermalhydraulic Simulations

D.R. Novog and J.S. Chang
Department of Eng. Physics, McMaster University, Hamilton, Ontario, Canada, L8S 4M1

The accuracy of heat transfer and pressure drop predictions in nuclear thermalhydraulic simulations directly effects both safety and operational analysis. Under high heat flux situations correlations established based on low heat flux experiments may not be extrapolated. In order to validate and extend existing correlations an experimental investigation has been conducted for high heat flux subcooled boiling heat transfer and pressure drop in a tubular channel. The data base (Novog et al. 1995) used to verify the existing correlations covered a mass flux range from 5 to 10 Mg/m²s, inlet temperature from 100 to 175°C, system pressure from 2.0 to 5.0 MPa and heat flux from 0.5 to 12 MW/m². The inside wall temperatures are calculated using outside wall temperature measurements and the one-dimensional radial conduction equation with internal heat generation. In the past, heat transfer analysis of high heat flux wall temperature measurements was based on a constant thermal conductivity solution. This paper presents the analytic and numerical simulation for inside wall temperatures based on variable thermal conductivity and compares these results to previous analysis. Comparisons were made between the present data and several existing correlations. The single-phase correlation from Pethukov et al. (1970) predicted the present results to within 25%. Satisfactory agreement was found with a modification of the Yin et al. (1993) high heat flux subcooled boiling correlation.

1. INTRODUCTION

The accurate prediction and modelling of nuclear thermalhydraulic behaviour is directly related to the heat transfer correlations used. Existing correlations based on low heat flux data are often extrapolated to many high heat flux situations. While the phenomenon of critical heat flux (CHF) or burnout has been the main focus for the most recent studies by Inasaka and Nariai[1], Araki et al.[2], Celata[3] and Yin et al.[4], subcooled boiling and single-phase high heat flux heat transfer and pressure drop have received less attention. Earlier studies conducted by Jens and Lottes[5] and Thom et al.[6] for boiling heat transfer are still being widely quoted in design analysis. Equation 1 shows the correlation from Jens and Lottes:

$$\Delta T_{SAT} = 25.0\,\phi^{0.25}\exp\left(\frac{-P}{62}\right) \qquad (1)$$

where T_{sat} is the temperature difference from saturation in °C, P is the system pressure in bars and ϕ is the heat flux in MW/m². Thom et al. modified the Jens and Lottes correlation to fit their data base for design purposes which is given by Equation 2:

$$\Delta T_{SAT} = 22.65\,\phi^{0.5}\exp\left(\frac{-P}{87}\right) \qquad (2)$$

More recently, Yin et al.[7] have experimentally investigated high heat flux subcooled boiling heat transfer for a water cooled channel under high heat flux conditions;

$$\Delta T_{SAT} = 7.195\,\phi\left(\frac{l}{L}\right)^{1.82} P^{-0.072} \qquad (3)$$

where l is the non-boiling length measured from the inlet of the heated section, L is the total heated length and P is the pressure in MPa. The ratio l/L shown in Equation 3 is limited by CHF conditions at that point. The strong thermal gradients may also affect the single-phase heat transfer coefficient and pressure drop.

Correlations based on a comprehensive data base does not exist for high heat flux single-phase and subcooled boiling heat transfer. This study was initiated to verify and extended the correlations used in the analysis of high heat flux systems. Furthermore, the analysis technique used to establish these correlations needs to be standardized and a proposed method is also included.

2. HIGH HEAT FLUX TESTING AND CONDITIONS

The high heat flux experimental test facility used by Novog et al.[8] is shown here. This recirculating loop can operate at a maximum pressure of 10 MPa, and is capable of supplying water up to 2 kg/s. The water flow rate was measured using a calibrated Venturi flow meter. A 50 kW preheater was capable of raising the water inlet temperature from 80 to 225 °C. The inlet and outlet water temperatures were measured using two resistive temperature devices (RTD). A 350 kW DC power supply was used to heat the test section. The present investigation covered water mass fluxes from 5 to 10 Mg/m²s, inlet temperatures from 100 to 175 °C and system pressures from 2 to 5 MPa.

To account for the accuracy and uncertainty of the heat flux measurements, a series of single-phase heat balance experiments were carried out using different flow rates, inlet temperatures and test section power levels. The combined uncertainties in the power, flow, water temperature measurements and heat loss from the test section were calculated based on the water enthalpy change and the power supplied to the test section. The maximum measured heat balance error was within an error band of +1.5%. To minimize the wall temperature measurement error, which may effect the inside wall temperature, T_{wi}, calculations three types of thermocouples were used. These included 0.25 mm, 0.5 mm O.D. sheathed, K-type thermocouples and 0.75 mm thick bare wire type junctions. High thermal

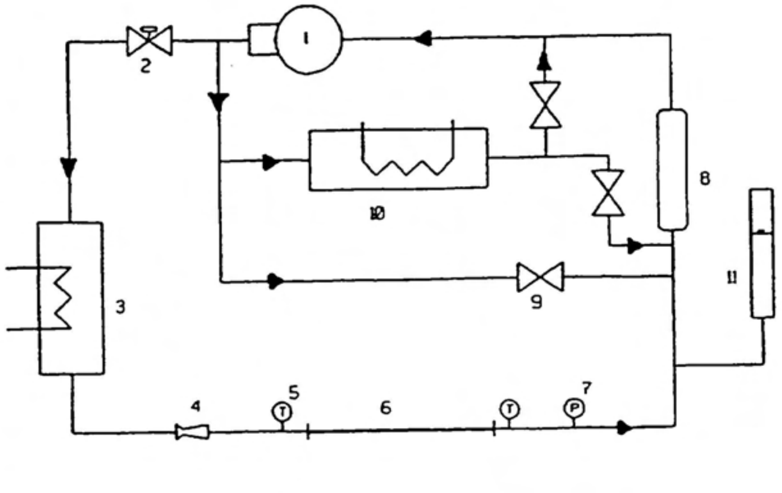

Figure 1 Schematic of High Pressure Water Boiling Water Flow Loop. (1. Circulation Pump, 2. Flow Control Valve, 3. Preheater, 4. Venturi Flow Meter, 5. RTD, 6. Test Section. 7. Outlet Pressure, 8. Condenser, 9. Bypass Valves, 10. Heat Exchanger, 11. Pressurizer).

conductivity cement and fibre-glass tape were used to pot these thermocouples to the test section outer wall. The accuracy and uncertainty of the wall temperature measurements were estimated to be within 2% of the absolute wall temperature based on several thermocouple measurements located at each axial position.

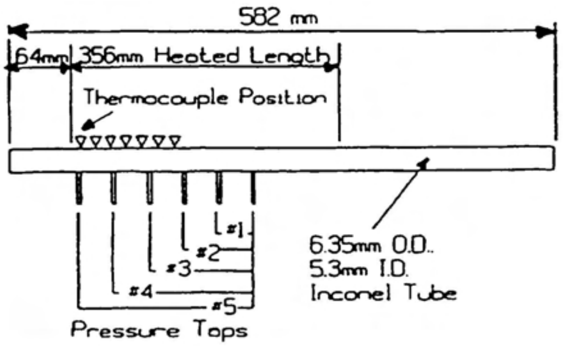

Figure 2 Schematic of Test Section, Thermocouple Layout and Pressure Tap Locations.

The test section was made from Inconel 600 tube with 6.33 mm outside diameter, 5.30 mm inside diameter and total length of 582 mm. Inconel was selected to ensure a uniform axial heat flux because the electrical resistivity remains nearly constant for the range of temperature variation along the 356 mm heated length. Fifteen thermocouples were attached to the heated section to measure the tube outer wall temperature at various axial and circumferential positions. The test section was thermally insulated to reduce heat loss to the environment. Figure 2 shows a schematic of the test section, the arrangement of wall thermocouples and pressure tap locations. These instruments were concentrated towards the test section outlet because high heat flux subcooled boiling first occurs in this region.

3. THERMAL CONDUCTIVITY EFFECTS

The calculation of inside wall temperatures was based on the one-dimensional thermal conductivity equation;

$$\frac{1}{r}\frac{d}{dr}\left(rK\frac{dT}{dr}\right) = q''' \tag{4}$$

where K is the thermal conductivity, T the temperature and q''' the thermal generation per unit volume resulting from Joule heating. The boundary equations for this system are;
i)constant outside wall temperature($T_R = T_{wo}$).
ii)perfect outer wall thermal insulation.

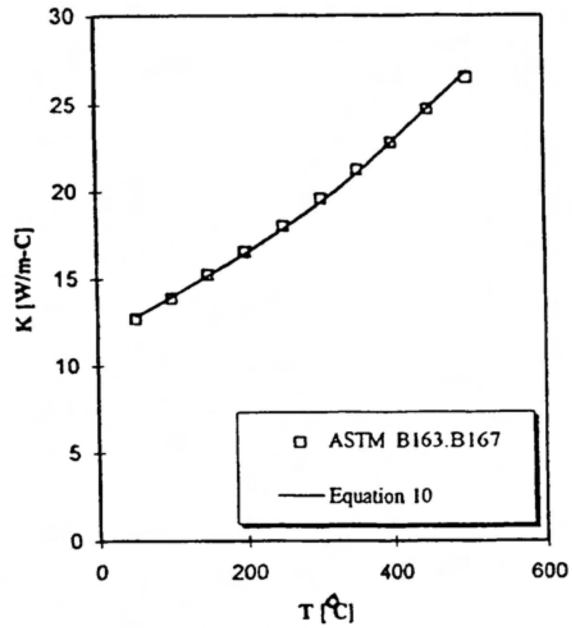

Figure 3 The Dependence of Thermal Conductivity on the Temperature of Inconel 600 (ASTM B163.B167) and Equation 10.

Previous analysis used for high heat flux experiments solved Equation 4 assuming a constant thermal conductivity and evaluated K at the average of the temperature profile[8]. However, the thermal conductivity of Inconel is a strong function of temperature as shown in Figure 3. This may lead to over estimation of inside wall temperatures. In order to more accurately estimate the inside wall temperatures, Equation 4 can be non-dimensionalized as follows;

$$\bar{r} = \frac{r}{R} \qquad \bar{T} = \frac{T}{T_R}$$
$$\bar{K} = \frac{K_T}{K_{T_R}} \qquad \bar{q} = \frac{q''' R^2}{K_{T_R} T_R} \qquad (5)$$

which then gives;

$$\frac{1}{\bar{r}} \frac{d}{d\bar{r}} \left(\bar{r} \bar{K} \frac{d\bar{T}}{d\bar{r}} \right) = \bar{q} \qquad (6)$$

Chang and Laframboise[9] have applied Kirchhoff transformations to heat conduction calculations in arbitrary shaped bodies. A similar transform in cylindrical coordinates between the inner and outer wall is;

$$\frac{dH}{d\bar{T}} = \bar{K} \; ; \quad H = \int_{\bar{T}}^{1} \bar{K} \, d\bar{T} \qquad (7)$$

Applying this transformation to Equation 6 yields;

$$\frac{1}{\bar{r}} \frac{d}{d\bar{r}} \left(\bar{r} \frac{dH}{d\bar{r}} \right) = \bar{q} \qquad (8)$$

The solution of Equation 7 with the transformed boundary conditions gives;

$$H = \frac{\bar{q}}{4} \left(\bar{r}^2 - 2\ln(\bar{r}) - 1 \right) \qquad (9)$$

Based on Figure 3 the variation of thermal conductivity with temperature can be approximated for Inconel 600 as follows;

$$K_T = K_0 \, e^{\omega T} \qquad (10)$$

where K_0 and ω are 11.8 W/m-K and 1.67×10^{-3} K^{-1} respectively. Integrating Equation 7 using Equation 10 yields;

$$H = \frac{1}{\omega T_R} \left(1 - e^{\omega T_R (\bar{T} - 1)} \right) \qquad (11)$$

Equating Equations 9 and 11 the non-dimensional temperature profile becomes;

$$\bar{T} = 1 + \frac{1}{\omega T_R} \times \ln\left(1 - \omega T_R \frac{\bar{q}}{4} \left(\bar{r}^2 - 2\ln(\bar{r}) - 1 \right) \right) \qquad (12)$$

In order to validate the above solution a one-dimensional radial finite difference solution, RADCON.FOR was constructed to solve Equation 4 and predict the inside wall temperatures. Expanding Equation 6 yields;

$$\frac{\bar{K}}{\bar{r}} \frac{d\bar{T}}{d\bar{r}} + \frac{d\bar{K}}{d\bar{r}} \frac{d\bar{T}}{d\bar{r}} + \bar{K} \frac{d^2\bar{T}}{d\bar{r}^2} = \bar{q} \qquad (13)$$

A finite difference solution was constructed based on Equation 13, the boundary conditions from above, and the thermal conductivity data shown in Figure 3. The first term derivative in Equation 13 was approximated as;

$$\frac{d\bar{T}}{d\bar{r}} \approx \frac{\bar{T}_{\bar{r}+\Delta\bar{r}} - \bar{T}_{\bar{r}}}{\Delta\bar{r}} \qquad (14)$$

The thermal conductivity gradient was

discreatized using;

$$\frac{d\bar{K}}{d\bar{r}} \approx \frac{\bar{K}_{\bar{r}+\Delta\bar{r}} - \bar{K}_{\bar{r}}}{\Delta\bar{r}} \tag{15}$$

The second derivative was approximated using a central difference about r;

$$\frac{d^2\bar{T}}{d\bar{r}^2} \approx \frac{\bar{T}_{\bar{r}+\Delta\bar{r}} + \bar{T}_{\bar{r}-\Delta\bar{r}} - 2\,\bar{T}_{\bar{r}}}{\Delta\bar{r}^2} \tag{16}$$

A total of 200 nodes were used between the inner and outer radius ($0.84 < r < 1.0$) with a convergence criteria of less than 0.01%.

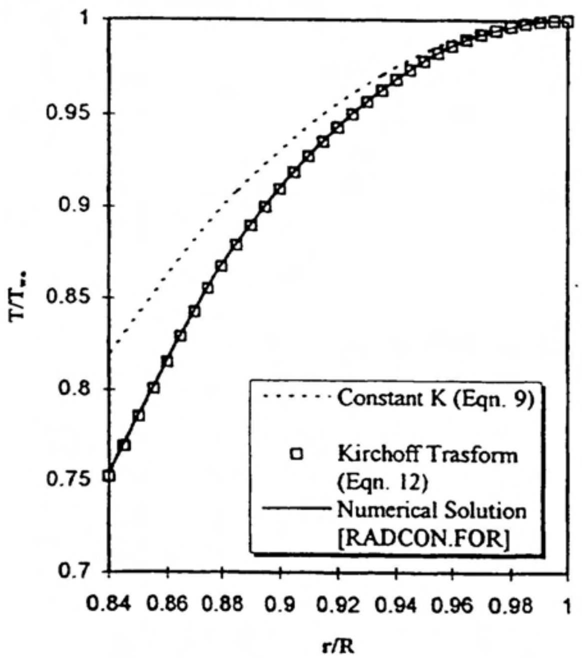

Figure 4 The Effect of Analysis Procedure on the Calculation of Inner Wall Temperatures at 42.5 MW/m².

Figure 4 shows the non-dimensional radial temperature profiles predicted using RADCON.FOR, Equation 12, and the constant thermal conductivity solution at a heat flux of 6.6 MW/m². The constant thermal conductivity solution over predicts the inside wall temperatures by more than 10% compared to the finite-difference and Kirchhoff transform methods. Equation 12 also shows that the difference between the constant thermal conductivity model and Kirchhoff transform solution increases with increasing heat flux. Hence Equation 12 was used to evaluate the inside wall temperature for calculating the inside wall temperatures based on outside wall temperature measurements.

All measurements were recorded using an on-line computer data acquisition system. For each series of tests the mass flux, G, inlet temperature, T_{IN}, and system pressure, P, were held constant while the electrical power to the test section was increased in 1 to 5 kW steps depending on the test conditions. Data was collected at all power levels after steady state was reached and each data point was averaged over a 15 second interval. The maximum power to the test section was limited to 70 kW by the wall temperature and burnout conditions. The heat flux to the test section was calculated by dividing the power supplied to the test section by the heated area based on the channel inside diameter and the effective heated length.

4. RESULTS AND DISCUSSION

The typical boiling curves obtained by Novog et al.[8] are reanalyzed based on the Kirchhoff transform solution and shown in Figure 5 where the test section heat flux is shown as a function of the channel inner wall temperature. The onset of nucleate boiling (ONB) is shown in Figure 5 as the kink in slope for each mass flux curve. For heat fluxes less than that corresponding to ONB the curve represents the single-phase convection regime. The steeper portion of the curve, above ONB, corresponds to subcooled nucleate boiling (SNB) regime. The effect of mass flux on the boiling curves is evident under a fixed system pressure of 3.5 MPa (T_{SAT} = 242 °C) and inlet temperature of 150

°C. Figure 5 shows that single-phase heat transfer increases with increasing mass flux. The subcooled boiling curves shown in Figure 5 converge together indicate that mass flux does not have a significant effect on SNB heat transfer. This resulted from the turbulence caused by rapid bubble departure and collapse during SNB overshadowing the mass flux contribution to heat transfer in this regime. Similar results were obtained for inlet temperatures of 100 and 150 °C.

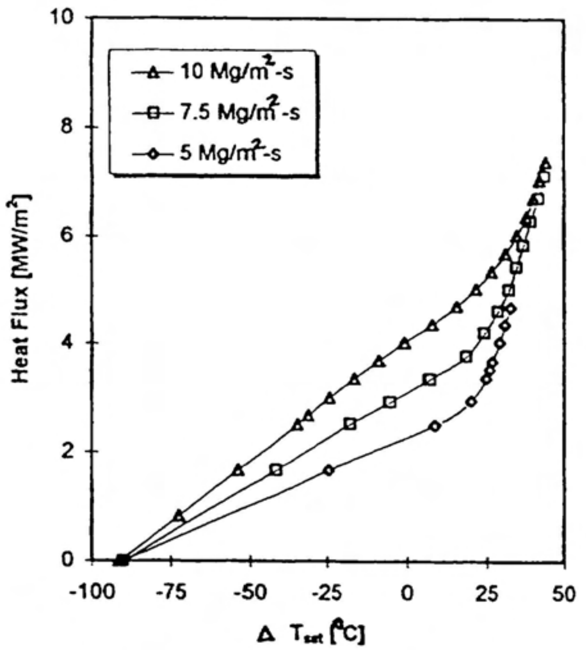

Figure 5 The Effect of Mass Flux on Subcooled Boiling Curves at an Inlet Temperature of 150 °C and 3.5 MPa.

The subcooled nucleate boiling results discussed above suggest that the mass flux and inlet temperature do not significantly affect SNB heat transfer. Figure 6 shows the SNB results for a selected range of mass flux and inlet temperatures covered in this study. The extrapolated correlations for the SNB heat transfer from Jens and Lottes[5] and Thom[6] are plotted along with the high flux correlation from Yin et al.[7] in Figure 6 for comparison. In the high flux region the agreement in wall temperature predictions and the measured values are within 20% in the case of Thom's correlation and near 200% from the Jens and Lottes' correlation. The SNB data from this experiment agrees quantitatively with the correlation from Yin et al. but significantly deviated at higher heat flux conditions. This may be due to Yin et al.'s calculation of inside wall temperatures which was based on a constant thermal conductivity profile. A modification to Yin et al.'s correlation which better predicts the present data is shown in Equation 17;

$$\Delta T_{SAT} = 12.4\, \phi^{0.75} \left(\frac{l}{L}\right)^{1.82} P^{-0.072} \qquad \textbf{(17)}$$

The scattering for the present study was within the typical uncertainties of highly subcooled boiling experiments. The physical properties used for data reduction and the wall temperature errors due to differences in the method of thermocouple attachment are considered the main sources of error.

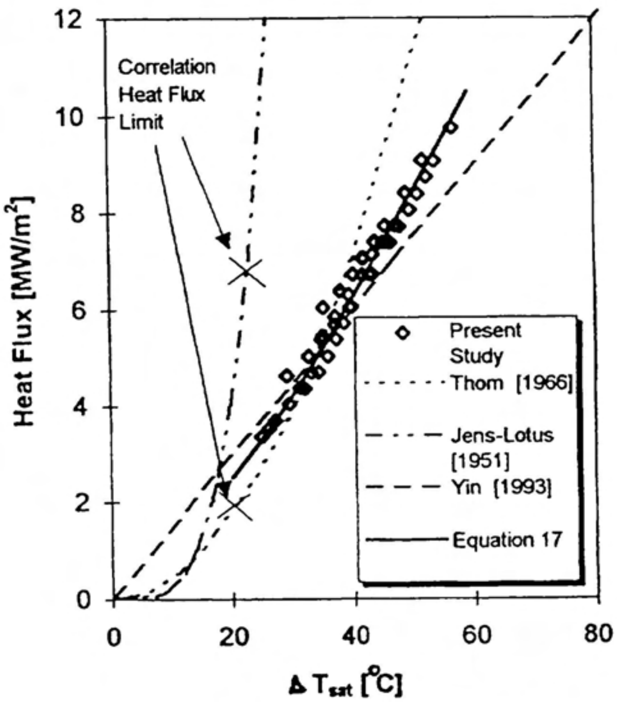

Figure 6 The Effect of High Heat Flux on Subcooled boiling Heat Transfer at 3.5 MPa.

Figure 7 shows the high heat flux single-phase heat transfer test results compared to existing correlations. The heat transfer coefficient is significantly over estimated by existing correlations from Dittus-Boelter[10] and Petukhov et al.[11]. Of these correlations Pethukov et al. predicted the present results to within 30%. The Pethukov et al. correlation was modified to fit the present data and is shown in Equation 18;

$$Nu = \frac{\left(\frac{f}{8}\right) Re\, Pr}{1.14 + 12.7\left(\frac{f}{8}\right)^{0.5}\left(Pr^{0.66} - 1\right)} \quad (18)$$

where f is the friction factor evaluated using the Blasius correlation for turbulent flow in pipes. The significant difference between the correlations and the present high heat flux investigation may be due to the large property variations caused by large temperature gradients near the tube wall.

The axial pressure drop from the inlet of the heated length are shown in Figure 8 as a function of the test section heat flux. The pressure drop decreases slightly as the heat flux increases up to the onset of nucleate boiling, after which further increasing the heat flux increases the pressure drop significantly. The decrease in the single-phase pressure drop may result from the drop in the water viscosity due to the higher temperatures in the wall region. The significant increase in the axial pressure drop for heat fluxes beyond ONB may result from the rapid creation and collapse of bubbles near the wall which increases the wall turbulence and hence the pressure drop.

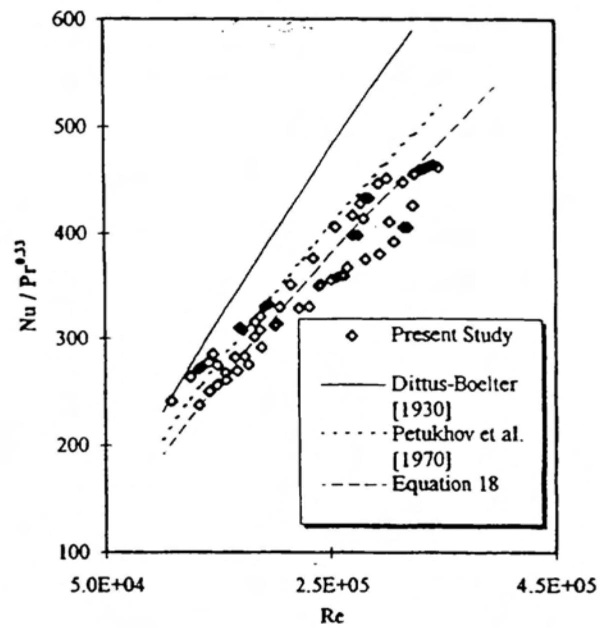

Figure 7 The Effect of Reynolds Number on Single-Phase Heat Transfer Under High Heat Flux Conditions at 3.5 MPa.

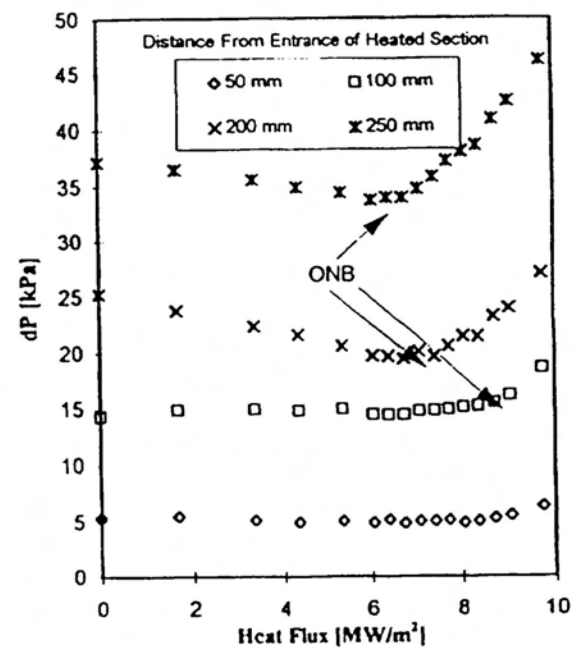

Figure 8 The Effect of Heat Flux on the Axial Pressure Drop at an Inlet Temperature of 125 °C and 3.5 MPa.

The single-phase friction factor is shown in Figure 9 for Reynolds numbers between 8×10^4 and 4×10^5 which was calculated from the pressure drop results at several axial locations. The results show that the Blasius correlation predicts the friction factor to within 30% for all heat flux conditions tested. The large data scatter shown in Figure 9 may result from buoyancy effects along the heated section caused by the high heat flux and large axial temperature gradients.

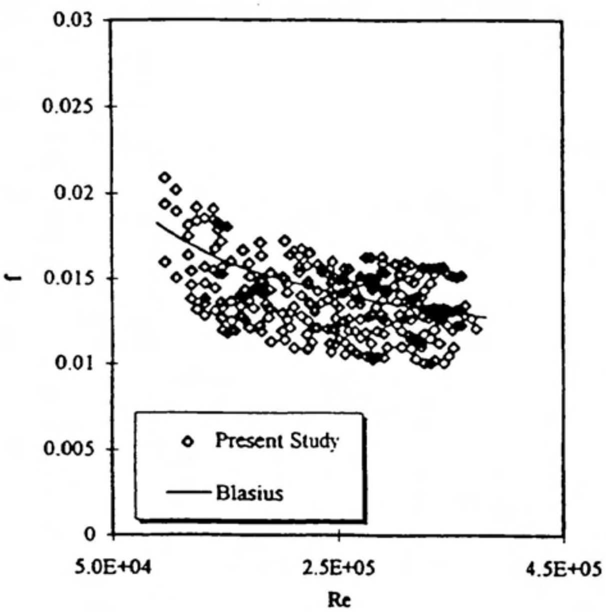

Figure 9 The Effect of Reynolds Number on Single-Phase Pressure Drop at 3.5 MPa.

5. CONCLUDING REMARKS

High heat flux subcooled boiling heat transfer and pressure drop correlations used in thermalhydraulic simulations have been investigated. The conclusions drawn from the present study are as follows;

1. The heat conduction analysis of high heat flux experimental data has been demonstrated using a Kirchhoff transform technique and was verified using a one-dimensional finite difference code. The discrepancy between previous data reduction methods and these solutions increased with increasing heat flux.
2. Existing subcooled nucleate boiling correlations based on much lower heat flux measurements give considerable under estimation of the present wall temperatures under high heal flux conditions. However, reasonable agreement was found between the present data base and a correlation derived by Yin et al. for high heat flux subcooled boiling.
3. The single-phase heat transfer coefficient was significantly affected by high heat flux conditions. The best existing correlation reviewed was from Pethukov et al. which predicted the single phase heat transfer results to within ±25%.
4. The axial pressure drop decreases with increasing heat flux up to the onset of nucleate boiling. After ONB the pressure drop increases significantly with increasing heat flux. The single-phase correlation from Blasius predicted the pressure drop results to within 20%. The significant amount of scatter in the friction factor data may result from the large axial temperature gradients caused by the high heat flux conditions.

Acknowledgments

The authors wish to acknowledge S.T. Yin, P. Gierszewski, D. Jackson, and V.S. Krishnan for their valuable discussions and comments. This work is supported by the Canadian Fusion Fuels Technology Project.

Nomenclature

D	= diameter
f	= friction factor
G	= mass flux
h	= heat transfer coefficient
I	= test section current
L	= total heated length
l	= length from heated section inlet
Nu	= Nusselt number
P	= system pressure
R	= test section resistance
r_{in}	= test section inside diameter
Re	= Reynolds number
T_{in}	= inlet water temperature
T_{out}	= outlet water temperature
T_{SAT}	= water saturation temperature
T_R	= test section outside wall temperature
ΔT_{sat}	= T_R - T_{SAT}
ϕ	= heat flux

References

1 F. Inaska and H. Nariai, *Critical heat flux of subcooled flow boiling water*, Procs. of 4th Int. Topical Meeting on Nuclear Reactor Thermalhydraulics, Oct.1989, pp. 111-120.

2 M. Araki et al., *Burnout experiments on the externally-finned swirl tube for steady state and high heat flux beam stops*, Fusion Eng. And Des., **9**, 1989, pp.231-236.

3 G.P. Celata, *A review of recent experiments and prediction aspects of burnout at very high heat fluxes*, Procs. of the International Conf. On Multiphase Flow, 1991, Tsukuba, Japan.

4 S.T. Yin, A. Cardella, A.H. Abdelmessih, Z. Jin, B.P. Bromley, *Assessment of a heat transfer package for water cooled plasma facing components in fusion reactors*, Nuc. Eng. and Design, **146**, p. 311, 1994.

5 W.H. Jens and P.A. Lottes, *Analysis of heat transfer, burnout, pressure drop and density data for high pressure water*, ANL-4621, Argonne National Laboratory, 1951.

6 J.R. Thom, W.M. Walker, T.A. Fallon, and G.F. Reising, *Boiling in subcooled water during flow up in heated tubes or Annuli*, Procs. of Inst. Of Mech. Eng., **180**, Part 3C, 1966.

7 Yin, S.T., Jin, Z., Abdelmessih, A.H., Gierszewski, P.J., "Prediction of highly subcooled flow boiling for cooling of high heat-flux components in fusion reactors", NURETH-6, Grenoble, Oct. 5-8, 1993.

8 Novog, D.R., Yin, S.T., Chang, J.S., "High Heat Flux Subcooled Boiling Heat Transfer and Pressure Drop Under Smooth- and Swirl-Flow Conditions", *ANS Procs. of 1995 National Heat Transfer Conference*, **8**, p. 139, 1995.

9 Chang, J.S., and Laframboise, J.G., *Int. Journal of Heat and Mass Transfer*, **38**, p. 360-362, 1978.

10 Dittus, F.W., and Boelter, L.M.K., University of California Publications on Engineering, Vol. 2, p. 443, Berkley, 1930.

11 Petukhov, B.S., Advances in Heat Transfer, Vol. 6, Irvine and Hartnett Editors, Academic Press, New York, 1970.